ЖЭТФ, 2008, том 134, вып. 5 (11), стр. 968–979

ORIGIN OF "HOT SPOTS" IN THE PSEUDOGAP REGIME OF $Nd_{1.85}Ce_{0.15}CuO_4$: AN LDA+DMFT+$\Sigma_{\mathbf{k}}$ STUDY

E. E. Kokorina [a], ***E. Z. Kuchinskii*** [a], ***I. A. Nekrasov*** [a*], ***Z. V. Pchelkina*** [b], ***M. V. Sadovskii*** [a**], ***A. Sekiyama*** [c], ***S. Suga*** [c], ***M. Tsunekawa*** [c]

[a] *Institute for Electrophysics, Russian Academy of Sciences 620016, Ekaterinburg, Russia*

[b] *Institute for Metal Physics, Russian Academy of Sciences 620219, Ekaterinburg, Russia*

[c] *Graduate School of Engineering Science, Osaka University, Toyonaka, Osaka 560-8531, Japan*

Received April 17, 2008

Material-specific electronic band structure of the electron-doped high-T_c cuprate $Nd_{1.85}Ce_{0.15}CuO_4$ (NCCO) is calculated in the pseudogap regime using the recently developed generalized LDA+DMFT+$\Sigma_{\mathbf{k}}$ scheme. The LDA/DFT (density-functional theory within local density approximation) provides model parameters (hopping integral values and local Coulomb interaction strength) for the one-band Hubbard model, which is solved by the DMFT (dynamical mean-field theory). To take pseudogap fluctuations into account, the LDA+DMFT is supplied with an "external" k-dependent self-energy $\Sigma_{\mathbf{k}}$ that describes interaction of correlated conducting electrons with nonlocal Heisenberg-like antiferromagnetic (AFM) spin fluctuations responsible for the pseudogap formation. Within this LDA+DMFT+$\Sigma_{\mathbf{k}}$ approach, we demonstrate the formation of pronounced "hot spots" on the Fermi surface (FS) map in NCCO, opposite to our recent calculations for $Bi_2Sr_2CaCu_2O_{8-\delta}$ (Bi2212), which have produced a rather extended region of the FS "destruction". There are several physical reasons for this fact: (i) the "hot spots" in NCCO are located closer to the Brillouin zone center; (ii) the correlation length ξ of AFM fluctuations is longer for NCCO; (iii) the pseudogap potential Δ is stronger than in Bi2212. Comparison of our theoretical data with recent bulk-sensitive high-energy angle-resolved photoemission (ARPES) data for NCCO provides good semiquantitative agreement. Based on that comparison, an alternative explanation of the van Hove singularity at -0.3 eV is proposed. Optical conductivity for both Bi2212 and NCCO is also calculated within the LDA+DMFT+$\Sigma_{\mathbf{k}}$ scheme and is compared with experimental results, demonstrating satisfactory agreement.

PACS: 71.10.Fd, 71.10.Hf, 71.27.+a, 71.30.+h, 74.72.-h

1. INTRODUCTION

There is a good reason to believe that proper description of the pseudogap regime is the avenue approaching the physical nature of high-T_c superconductivity [1]. Angle-resolved photoemission spectroscopy (ARPES) has been coming along this way very well in recent years. One of the test compounds for ARPES is the hole-doped $Bi_2Sr_2CaCu_2O_{8-\delta}$ (Bi2212) system. Another example is the electron-doped high-T_c compound $Nd_{2-x}Ce_xCuO_4$ (NCCO). There are numerous experimental ARPES data on Bi2212 and NCCO (see review [2]). Fermi surface (FS) maps, quasiparticle band dispersions, and even self-energy lineshapes within mapping on some models are reliably extracted from modern ARPES data [2].

There are several interesting physical phenomena associated with the pseudogap regime (in the normal underdoped phase): a partial "destruction" of the FS and folding of band dispersions (shadow bands) for both compounds Bi2212 and NCCO [2]. Despite evi-

*E-mail: nekrasov@iep.uran.ru
**E-mail: sadovski@iep.uran.ru

dent similarities of experimental observations for these two systems, there is one striking distinction. The FS of Bi2212 has so-called Fermi "arcs" around the $(\pi/2,\pi/2)$ point (looking like a part of a noninteracting FS), but the sharply defined FS just vanishes towards the Brillouin zone (BZ) borders. In its turn, NCCO also has slightly degraded Fermi "arcs", but the noninteracting FS is almost restored in the vicinity of BZ borders. In between, there are well known "hot spots"—areas of FS "destruction" around the points where the FS intersects the umklapp BZ border. These "hot spots" are not observed so obviously for Bi2212. The aim of this paper is to show the origin of this NCCO "hot-spot" behavior.

At moderate doping, both systems under consideration are usually treated as Mott insulators or, in other words, as strongly correlated metals. The modern technique to solve the Hubbard model is the dynamical mean-field theory (DMFT), which is exact in infinitely many dimensions [3]. However, the quasi-two-dimensional nature of high-T_c compounds is well known. To overcome the local nature of the DMFT approximation, we recently proposed a semiphenomenological DMFT+$\Sigma_{\mathbf{k}}$ computational scheme [4–6], where an additional self-energy $\Sigma_{\mathbf{k}}$ describes nonlocal correlations induced by (quasi)static short-range collective Heisenberg-like antiferromagnetic (AFM) spin (pseudogap) fluctuations [7, 8]. Assuming the additive form of the self-energy within the DMFT+$\Sigma_{\mathbf{k}}$ approach, we can preserve the conventional DMFT self-consistent set of equations. To take material-specific properties of both Bi2212 and NCCO into account, we perform first-principle one-electron density functional theory calculations within local density approximation (DFT/LDA) [9]. The LDA results are then incorporated into DMFT+$\Sigma_{\mathbf{k}}$ in accordance with the LDA+DMFT ideology [10]. To solve the effective single-impurity problem of the DMFT, we use the reliable numerical renormalization-group approach (NRG) [11, 12]. Such a combined LDA+DMFT+$\Sigma_{\mathbf{k}}$ scheme is by construction particularly suitable for the description of electron properties of real high-T_c materials at finite doping in the normal state.

The DMFT+$\Sigma_{\mathbf{k}}$ approach was extensively used recently to describe formation of a pseudogap in the strongly correlated metallic regime of the single-band Hubbard model on a square lattice [4–6]. We have also generalized the DMFT+$\Sigma_{\mathbf{k}}$ approach to account for static disorder effects [6]. Later, we derived the DMFT+$\Sigma_{\mathbf{k}}$ approach to calculate two-particle properties (such as the optical conductivity) [13]. We recently used DMFT+$\Sigma_{\mathbf{k}}$ to analyze the general problem of the metal–insulator transition in strongly disordered and strongly correlated systems [14].

The LDA+DMFT+$\Sigma_{\mathbf{k}}$ scheme has already been used to describe the pseudogap regime in "realistic" calculations for Bi2212 [15]. In this paper, we apply this approach to NCCO with the aim to describe the characteristic differences of its electron structure compared to Bi2212.

This paper is organized as follows. In Sec. 2, we present a short introduction into the *ab initio* self-consistent generalized combined LDA+DMFT+$\Sigma_{\mathbf{k}}$ scheme and its extension taking two-particle properties (optical conductivity) into account. Section 3 contains Bi2212 and NCCO material-specific information: the LDA-calculated band structure, Fermi surfaces, and details on some model-parameter calculations. Results and discussion of the LDA+DMFT+$\Sigma_{\mathbf{k}}$ calculations for Bi2212 and NCCO and comparison with experimental data are presented in Sec. 4. Section 5 concludes this paper with a summary and discussion of some remaining problems.

2. COMPUTATIONAL METHOD

To introduce a spatial length scale (nonlocal correlations) into the conventional DMFT method [3], we recently proposed the generalized DMFT+$\Sigma_{\mathbf{k}}$ approach [4–6], with the computational scheme shown in Fig. 1, which contains the flow diagram of a self-consistent DMFT+$\Sigma_{\mathbf{k}}$ set of equations. First, we guess some initial local (DMFT) electron self-energy $\Sigma(i\omega)$. Second, we compute (by any available technique for the chosen model) the $\mathbf{k}$-dependent "external" self-energy $\Sigma_{\mathbf{k}}(i\omega)$, which can be a functional of $\Sigma(i\omega)$ in general. Then, neglecting the interference effects between the self-energies (which in fact is the major assumption of our approach), we can set up and solve a lattice problem of the DMFT (step 3 in Fig. 1). At step 4, we then define an effective Anderson single-impurity problem, which is to be solved by any "impurity solver" to close the DMFT+$\Sigma_{\mathbf{k}}$ equations.

The additive form of self-energy (at step 3 in Fig. 1) is in fact an advantage of our DMFT+$\Sigma_{\mathbf{k}}$ approach [4–6]. It allows preserving the set of self-consistent equations of the standart DMFT [3]. However, there are two distinctions from the conventional DMFT. During each DMFT iteration, we recalculate the corresponding $\mathbf{k}$-dependent self-energy $\Sigma_{\mathbf{k}}(\mu,\omega,[\Sigma(\omega)])$ within some (approximate) scheme, e.g., taking interactions with collective modes or order parameter fluctuations into account, and the local Green's function $G_{ii}(i\omega)$ is "dressed" by $\Sigma_{\mathbf{k}}$ at each step. When the

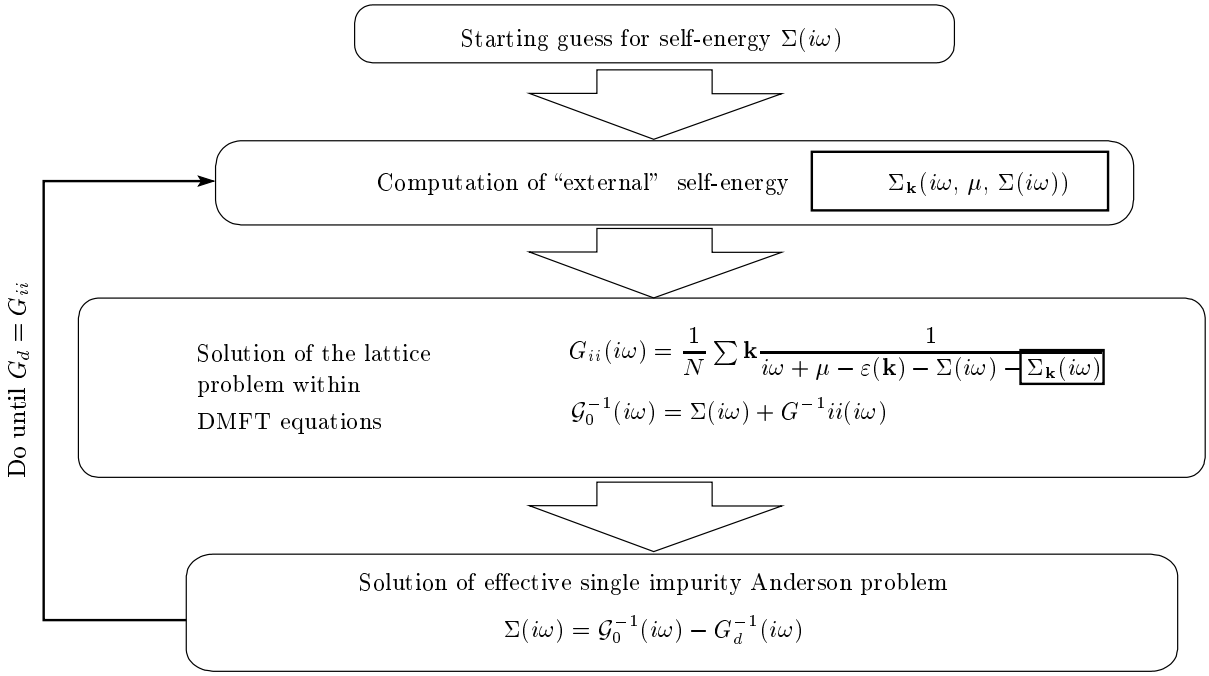

Fig. 1. Flow diagram of the DMFT+$\Sigma_{\mathbf{k}}$ self-consistent loop; ii corresponds to lattice-problem and d to impurity-problem variables

input and output Green's functions (or self-energies), converge to each other (with prescribed accuracy), we consider the obtained solution self-consistent. Physically, this corresponds to the account of some "external" (e.g., pseudogap) fluctuations, characterized by an important length scale ξ, into the fermionic "bath" surrounding the effective Anderson impurity of the usual DMFT.

In the present work, $\Sigma_{\mathbf{k}}(\omega)$ represents interaction of a correlated electron with antiferromagnetic (AFM) pseudogap fluctuations. To calculate $\Sigma_{\mathbf{k}}(\omega)$ in the case of random field of pseudogap fluctuations (assumed to be (quasi)static and Gaussian, which is valid at sufficiently high temperatures [7, 8]) with the dominant scattering momentum transfers of the order of the characteristic vector $\mathbf{Q} = (\pi/a, \pi/a)$ (where a is the lattice constant), typical of the AFM fluctuations ("hot-spot" model [1]), we use the recursion procedure proposed in Refs. [7, 8, 16], with material-specific generalizations as described in detail in Refs. [15].

There are two important parameters characterizing the pseudogap regime in our scheme: the pseudogap energy scale (amplitude) Δ and the spatial correlation length ξ [8, 15]. Actually, we prefer to take Δ and ξ determined somehow from experiment. However, we can also use certain model estimates to calculate them microscopically [5]. Both approaches are used below.

To calculate the optical conductivity, we use our generalization of DMFT+$\Sigma_{\mathbf{k}}$ for calculation of two-particle properties (vertex parts) as described in detail in Ref. [13], with material-dependent parameters provided by LDA+DMFT+$\Sigma_{\mathbf{k}}$ and vertex corrections due to pseudogap fluctuations calculated using the recursion relations derived in Ref. [17]

3. LDA BANDS AND FS OF NCCO AND Bi2212, EFFECTIVE MODEL PARAMETERS

As the first step of our LDA+DMFT+$\Sigma_{\mathbf{k}}$ hybrid scheme, we perform LDA band structure calculations. For both compounds, the ideal tetragonal bcc crystal lattice with the space symmetry group $I4/mmm$ is reported (see Ref. [18] for Bi2212 and Ref. [19] for NCCO). The physically relevant structural motif for high-T_c materials is the CuO_2 plane. There are two CuO_2 planes displaced close to each other in the unit cell of Bi2212, and just one such plane for NCCO. We have done LDA calculations of the electron band structure within the linearized muffin-tin orbital (LMTO) basis set [20]. The results are presented as thin lines in Fig. 2. Our band structures agree well with previous works Ref. [21] and Ref. [22] for Bi and Nd compounds respectively.

Calculated energy model parameters for Bi2212 and NCCO (eV). The first four Cu–Cu in-plain hopping integrals t, t', t'', t''', the interplain hopping value $t_\perp$, the local Coulomb interaction U, and the pseudogap potential Δ

	t	t'	t''	t'''	$t_\perp$	U	Δ
Bi2212	−0.627	0.133	0.061	−0.015	0.083	1.51	0.21
NCCO	−0.44	0.153	0.063	−0.0096	–	1.1	0.36

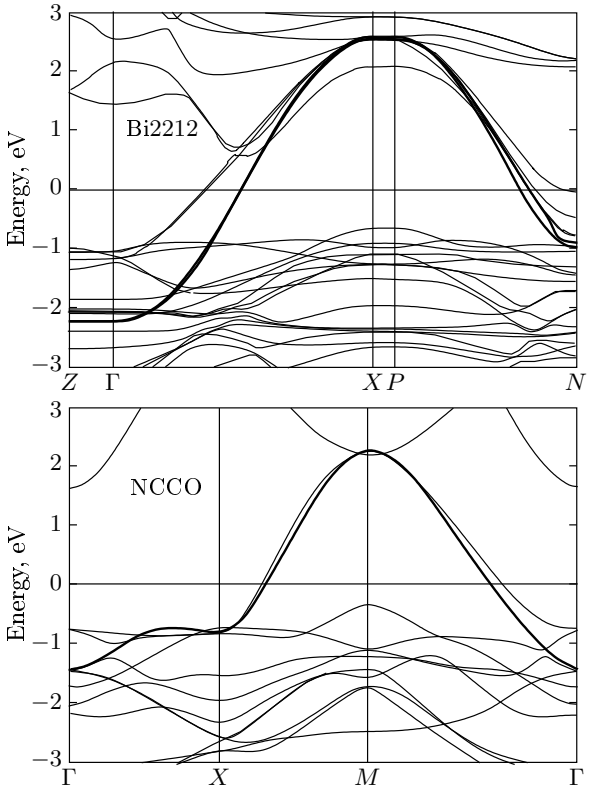

Fig. 2. LDA bands (thin lines) for Bi2212 (left) and NCCO (right) along the BZ high-symmetry directions. For both panels, thick lines correspond to the effective x^2-y^2 symmetry Wannier-like state dispersions. Zero energy corresponds to the Fermi level

To calculate hopping integral values for the Bi system, we used the Wannier-function projecting method [23] in the LMTO framework [24]. Hopping integrals of the Nd compound were obtained by using the so-called NMTO method [25] (see Table). Values of hopping integrals computed by these two methods agree well for the respective compounds [26]. In Fig. 2, the thick line shows the dispersion of the effective x^2-y^2 Wannier-like orbital that crosses the Fermi level and is most interesting physically. These dispersions correspond to hopping integral values (tight-binding parameters) given in the Table.

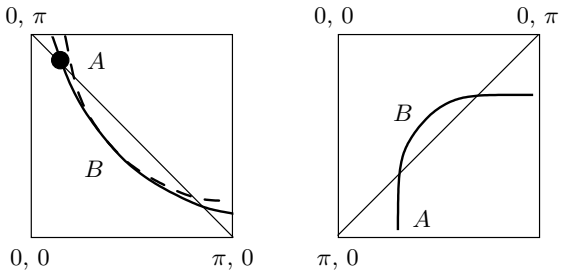

Fig. 3. LDA-calculated Fermi surfaces for Bi2212 (left) and NCCO (right) in a quarter of the BZ. Diagonal line corresponds to the (AFM) umklapp scattering surface

Figure 3 contains noninteracting LDA Fermi surfaces (FS) in the (k_x, k_y) plane for a quarter of the first BZ. The shape of these FS is defined by the tight-binding parameters in the Table. The diagonal line corresponds to the AFM-folded BZ border. In the left panel for Bi2212, we can see two FS sheets. This is caused by finite hopping between two neighboring CuO_2 layers, the so-called bilayer splitting. The value $t_\perp$ is given in the Table. The simplest tight-binding expression for the bilayer splitting derived in [27] is used in our calculations (see Ref. [15] for the details).

It is important to note the "hot-spot" positions (intersections of the FS with the AFM umklapp surface) for both materials. It is $(0.47,2.66)\pi/a$ for Bi2212 and $(0.95,2.19)\pi/a$ for NCCO, whence we can see that the "hot spots" are located farther away from the BZ border in NCCO than in Bi2212. We recall that pseudogap fluctuations scatter electrons from the vicinity of one "hot spot" to the vicinity of another, i.e., by the scattering vector of the order of $\mathbf{Q}$. The effective scattering area around the "hot spot" is determined by the inverse correlation length ξ^{-1} of these fluctuations. We also recall that the $(\pi/a,0)$ point is surrounded by four BZ from different sides. Consequently, if a "hot spot" is closer to $(\pi/a,0)$ and ξ is small enough, the FS is "destroyed" in a rather wide region close to the BZ border crossings. We can therefore expect "hot spots" to be

observed more explicitly for NCCO, while the part of the FS close to the BZ border crossings be less affected by pseudogap fluctuations in contrast to Bi2212.

The values of the local Coulomb interaction U for the x^2-y^2 orbital were obtained by a constrained LDA method [28] (see the Table for the values). These values are of the order of 2–3t for both systems. It is in fact quite a bit smaller than the values many people believe should be used in model calculations (usually about 4–6t; see, e.g., Ref. [29]). We note that due to a different orbital set that provides screening of the Coulomb interaction value U on the Cu-3d shell for the problem under discussion, we obtain smaller values of U in comparison, e.g., with Ref. [26]. At the same time, our previous experience with constrained LDA computations shows that they give reasonable estimates for the U value in a number of other oxides [30]. However, to further analyze the influence of the U value on observable quantities, we performed additional LDA+DMFT+$\Sigma_{\mathbf{k}}$ computations for increased values of U. A short discussion of the results is given in Sec. 5. The values of Δ for both systems were calculated as proposed in Ref. [5] (the Table) (see the Appendix for more details). The correlation length ξ was taken from experiments, i.e., $\xi \sim 10a$ for Bi2212 [1] and $\xi \sim 50a$ for NCCO [31].

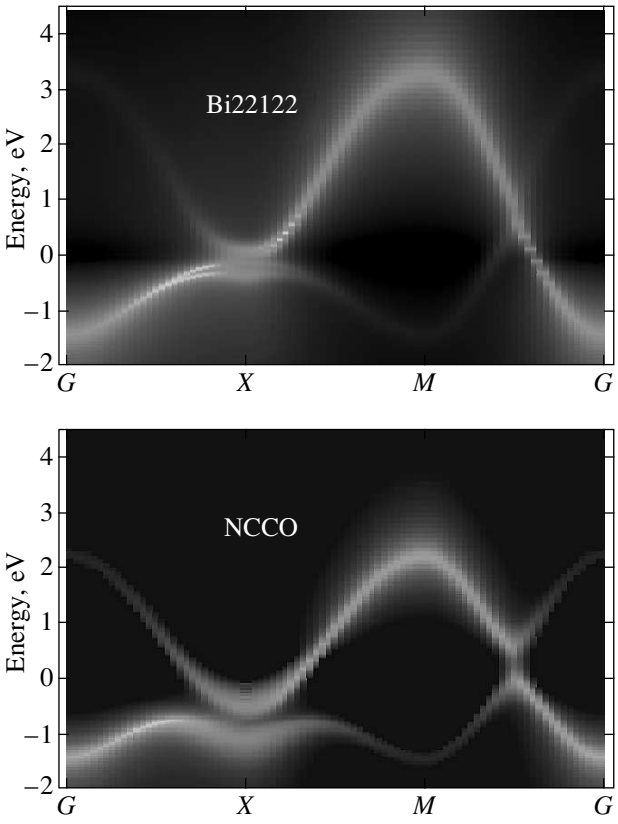

Fig. 4. LDA+DMFT+$\Sigma_{\mathbf{k}}$ spectral functions contour plot for Bi2212 (upper panel) and NCCO (lower panel) along the BZ high-symmetry directions of the first BZ $\Gamma(0,0) - \mathrm{X}(\pi,0) - \mathrm{M}(\pi,\pi) - \Gamma(0,0)$. Zero energy corresponds to the Fermi level

4. NCCO VS. Bi2212 LDA+DMFT+$\Sigma_{\mathbf{k}}$ RESULTS AND EXPERIMENTAL DATA

A. Quasiparticle Dispersions

Finite temperatures and interactions lead to finite life-time effects in general. Therefore, instead of quasiparticle dispersions expressed by the usual dispersion curves (as in DFT/LDA, for example), in Fig. 4 we display contour plots of the corresponding spectral functions $A(\omega, \mathbf{k})$:

$$A(\omega, \mathbf{k}) = -\frac{1}{\pi} \operatorname{Im} G(\omega, \mathbf{k}), \qquad (1)$$

where $G(\omega, \mathbf{k})$ is the retarded Green's function obtained via our LDA+DMFT+$\Sigma_{\mathbf{k}}$ scheme (shown in Fig. 1) with an appropriate analytic continuation to real frequencies.

Prima facie, both compounds Bi2212 (the upper panel in Fig. 4) and NCCO (the lower panel in Fig. 4) have similar quasiparticle bands. There are two bands in each case instead of just one in the case of DFT/LDA. Of these, the broadest and most intensive band predominantly follows the noninteracting DFT/LDA band (see Fig. 2). The second band in our case is an AFM-like reflex (shadow band) of the DFT/LDA band and is much less intensive. This is a direct effect of the self-energy $\Sigma_{\mathbf{k}}$ due to pseudogap fluctuations introduced into the conventional DMFT scheme (see Ref. [32] for discussion).

As discussed above, finite life-time (interaction) effects should be especially strong around the (π/a,0) point (the X point in Fig. 4). This is clearly visible in both panels of Fig. 4. However, we showed in Sec. 3 that the Bi2212 "hot spot" is much closer to the X point. We thus see a large quasiparticle band broadening on the Fermi level (we must not forget bilayer splitting effects). For NCCO, there is no sizeable broadening on the Fermi level close to the X point. Both branches go below the Fermi level at about -0.5 eV. In NCCO, the Fermi "arc" is much closer to the umklapp surface, and hence the pseudogap effects are significant around the ($\pi/2a$,$\pi/2a$) point (the middle point of the $\Gamma - M$ direction) in contrast to Bi2212.

Figure 5 shows changes from the effective $x^2 - y^2$ LDA bands (upper panel) to the LDA+DMFT+$\Sigma_{\mathbf{k}}$

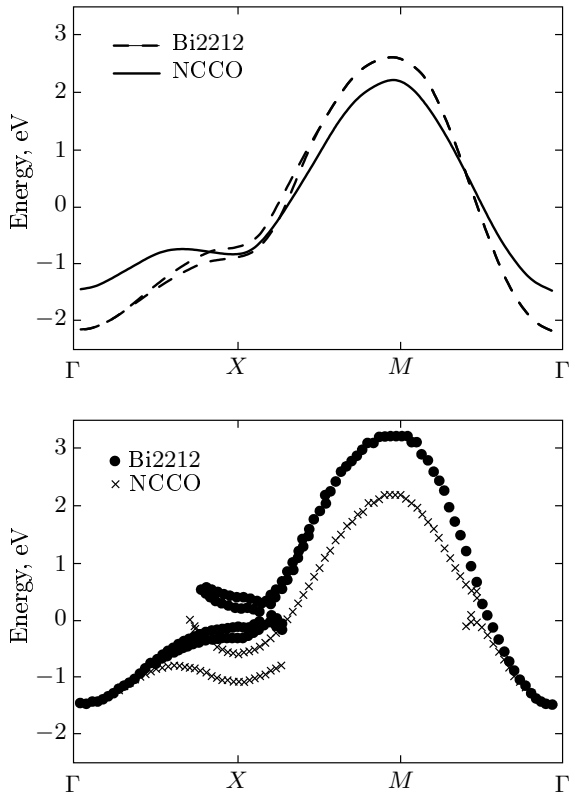

Fig. 5. Comparison of the effective LDA x^2-y^2 bands (upper panel) and the LDA+DMFT+$\Sigma_{\mathbf{k}}$ quasiparticle dispersions (lower panel) for Bi2212 and NCCO along the BZ high-symmetry directions. Zero energy corresponds to the Fermi level

quasipartical bands (lower panel) for both Bi2212 and NCCO. Quasiparticle bands on the lower panel in Fig. 5 represent the positions of the maxima of spectral functions shown in Fig. 4. In Bi2212, the shadow band and the quasiparticle band intersect each other at the "hot spot" close to the X point. In NCCO, there is no such intersection, but the shadow and quasiparticle bands are quite parallel around the X point. Close to $(\pi/2a,\pi/2a)$, we observe a kind of precursor of the dielectric AFM gap. Nothing of that sort is observed for Bi2212. We also note that the calculated shadow band is actually an order of magnitude less intensive in Bi2212 than in NCCO.

B. Spectral Functions

Figure 6 displays LDA+DMFT+$\Sigma_{\mathbf{k}}$ spectral functions (1) along a 1/8 of the noninteracting FS from the nodal point (top curve) to the antinodal one (bottom curve) (the respective points A and B in Fig. 3). Data for Bi2212 are given in the left panel, and for NCCO in the right panel in Fig. 6. For both compounds, the antinodal quasiparticles are well-defined, shown by a sharp peak close to the Fermi level. In approaching the nodal point, the quasiparticle damping increases and the peak shifts towards higher binding energies. This behavior is confirmed by experiments in Refs. [33, 34] (see Ref. [35] for a brief comparison with experiment). Again, there are some differences between these two compounds. As we have noted, "hot spots" for NCCO are closer to the BZ center. In Fig. 5, we can see this from the position of the dashed line, which corresponds to the "hot-spot" $\mathbf{k}$-point. Thus another explanation of the peaks can be given. Namely, for Bi2212, nodal quasiparticles are formed by the low-energy edge of the pseudogap and for NCCO, they are formed by the higher-energy pseudogap edge. Also, there are obviously no bilayer splitting effects in NCCO that are seen for Bi2212 (left panel in Fig. 6).

C. Comparison with ARPES Data

In Fig. 7, the LDA+DMFT+$\Sigma_{\mathbf{k}}$ FS maps on a quarter of the BZ for Bi2212 (upper left) and NCCO (upper right) are presented. The upper parts of Fig. 7 are just a contour plot of the spectral functions in Fig. 6. The above-mentioned significant FS "destruction" occurring because of pseudogap fluctuations close to the BZ borders is clearly seen for Bi2212. On the contrary, the NCCO FS is almost restored in the vicinities of the BZ border. Vice versa, a Fermi "arc" is quite sharp for Bi2212 and is rather degraded for NCCO. That is again a consequence of the "hot spots" being closer to the BZ center for NCCO. A slightly larger value of the pseudogap potential Δ also works towads the Fermi "arc" smearing in NCCO. It is significant to say that shadow FS are come to hand. The shadow FS is found to be more intensive for NCCO.

Qualitatively speaking, very similar FS shapes are observed experimentally for both Bi (Ref. [36]) and Nd (Ref. [33]) compounds (lower parts of Fig. 7). In our opinion, such FS maps have a material-specific origin. The LDA-calculated FS of NCCO has a larger curvature (left panel of Fig. 3) and intersects the BZ boundary away from the $(\pi/a,0)$ point, thus remaining nearly noninteracting, but the Bi2212 FS approaches the BZ border much closer to the $(\pi/a,0)$ point (right panel of Fig. 3). Therefore, "hot spots" are not seen in Bi2212. They are spread by strong pseudogap scattering processes near the $(\pi/a,0)$ point. A larger correlation length for NCCO is also favorable for more evident "hot spots".

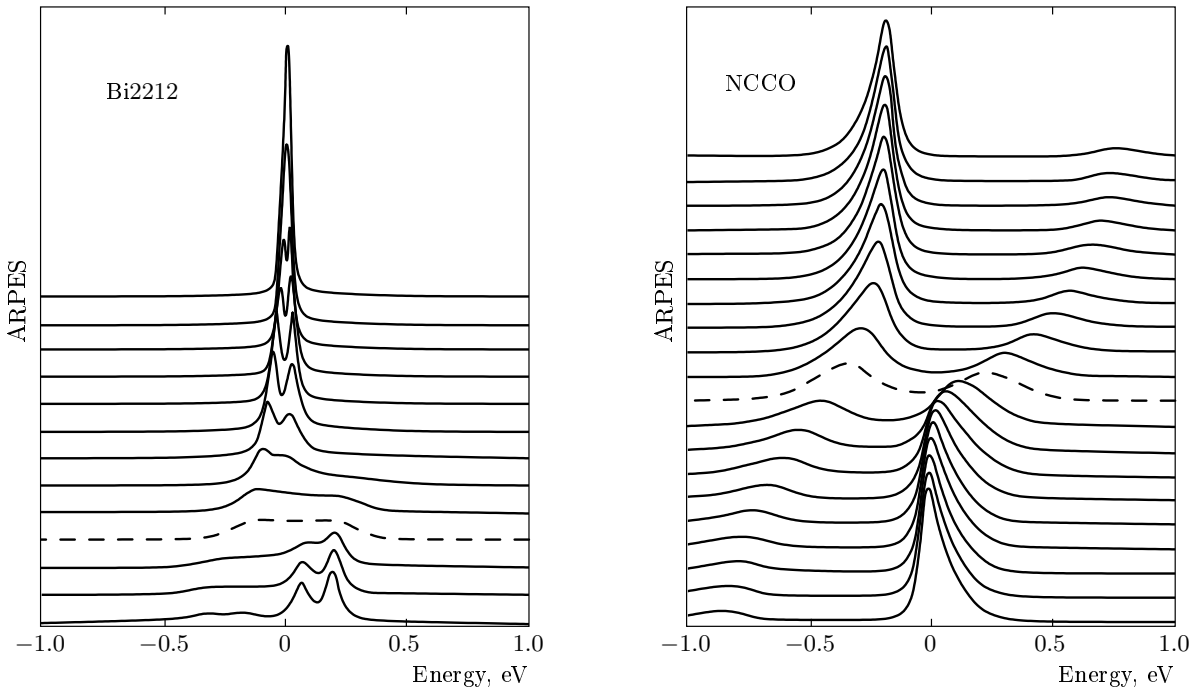

Fig. 6. LDA+DMFT+$\Sigma_{\mathbf{k}}$ spectral functions for Bi2212 (left panel) and NCCO (right panel) along the noninteracting FS in a 1/8 of the BZ. The dashed line corresponds to "hot spots"

In Fig. 8, we present the LDA+DMFT+$\Sigma_{\mathbf{k}}$ data in comparison with the recent high-energy bulk-sensitive angle-resolved photoemission data for $Nd_{1.85}Ce_{0.15}CuO_4$. For the details of experiment, we refer the reader to Ref. [37]. The lower panel of Fig. 8 shows intensity plots along the high-symmetry lines for NCCO obtained by high-hν ARPES. The upper panel in Fig. 8 is part of Fig. 4. To obtain a better agreement with this ARPES experiment, we changed the theoretical Fermi level by 0.2 eV.

We see quite a good agreement between the LDA+DMFT+$\Sigma_{\mathbf{k}}$ and experimental data. For the $M-\Gamma$ direction, there is not very much going on. Basically, we see a very intensive quasiparticle band both in theory and in experiment. For the $M-\Gamma$ direction, the low-intensity shadow band is not resolved in experiment.

A more interesting situation is observed for $\Gamma-X-M$ directions. At the Γ point, there is a band in the experiment starting at about -1.2 eV. It is rather intensive and increases in energy. Suddenly, the intensity becomes almost zero at about -0.3 eV. Then in the vicinity of the X point, the intensity again increases. In the $X-M$ direction, around -0.3 eV on the right side of the X point, there is also a region of quite high intensity. At a first glance, this may seen to be the same band with matrix element effects governing the intensity. But looking at the right panel in Fig. 5 (see the corresponding discussion in Sec. 4A), we can realize that this low-intensity region is the forbidden gap between shadow and quasiparticle bands. The "horseshoe" around the X point is formed by the shadow band on the left and the quasiparticle band on the right for the upper branch and other way round for the lower branch. This is also easily seen in Fig. 4 and the upper panel in Fig. 8. Consequently, there are also intensive shadow FS sheets around the $(\pi/a,0)$ point in Fig. 7 (upper right panel). Rather intensive nondispersing states at about -1.0 eV within the experimental data can be presumably associated with the lower Hubbard band and a possible admixture of some oxygen states. We also suppose that the high intensity at -0.3 eV for the X point may be interpreted as a van Hove singularity not of the bare dispersion [22] but of the high-energy pseudogap branch.

D. Comparison with Optical Data

Our recent generalization of the LDA+DMFT+$\Sigma_{\mathbf{k}}$ scheme incorporating two-particle properties [13] allows analyzing optical conductivity of the Bi and Nd

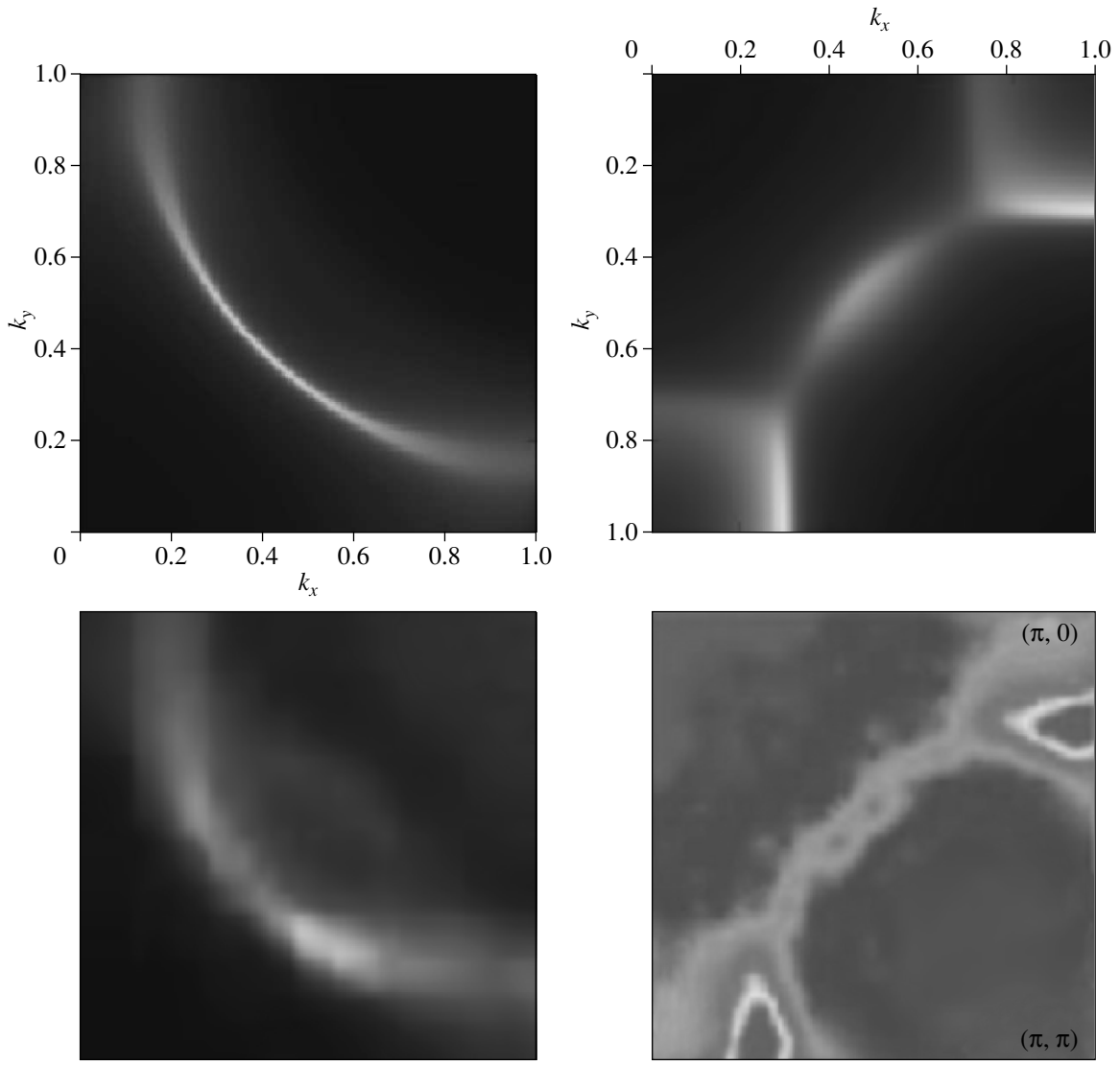

Fig. 7. LDA+DMFT+$\Sigma_{\mathbf{k}}$ Fermi surfaces for Bi2212 (upper left panel) and NCCO (upper right panel) in a 1/4 of the BZ (k_x and k_y are in units of π/a). The experimental FS for Bi2212 (lower left panel, Ref. [36]) and NCCO (lower right panel, Ref. [33])

materials under consideration. In Fig. 9, we compare experimental data with part of optical conductivities for NCCO (left panel) and Bi2212 (right panel). The way of computation is described above. Here, we can report qualitative agreement between our theoretical curve for NCCO with the calculated $\Delta = 0.36$ eV (solid line) and experiment [38]. Nevertheless, we find the calculated pseudogap value to be overestimated. To improve the agreement, we also calculated optical conductivity for the experimental value $\Delta = 0.2$ eV [38] (Fig. 9, dashed line). Concerning the Bi2212 optical conductivity (Fig. 9, right panel), we note that there is no particular structure either in the theory or in the experimental data [39]. For Bi2212, the agreement between experimental and theoretical curves is reasonable. We note that according to our calculations of the quasiparticle bands, spectral functions and FS maps are not strongly modified for $\Delta = 0.2$ eV.

E. Influence of the U Value on DMFT+$\Sigma_{\mathbf{k}}$ Results

Before we summarize our results, we discuss how the Hubbard interaction U value affects the DMFT+$\Sigma_{\mathbf{k}}$ re-

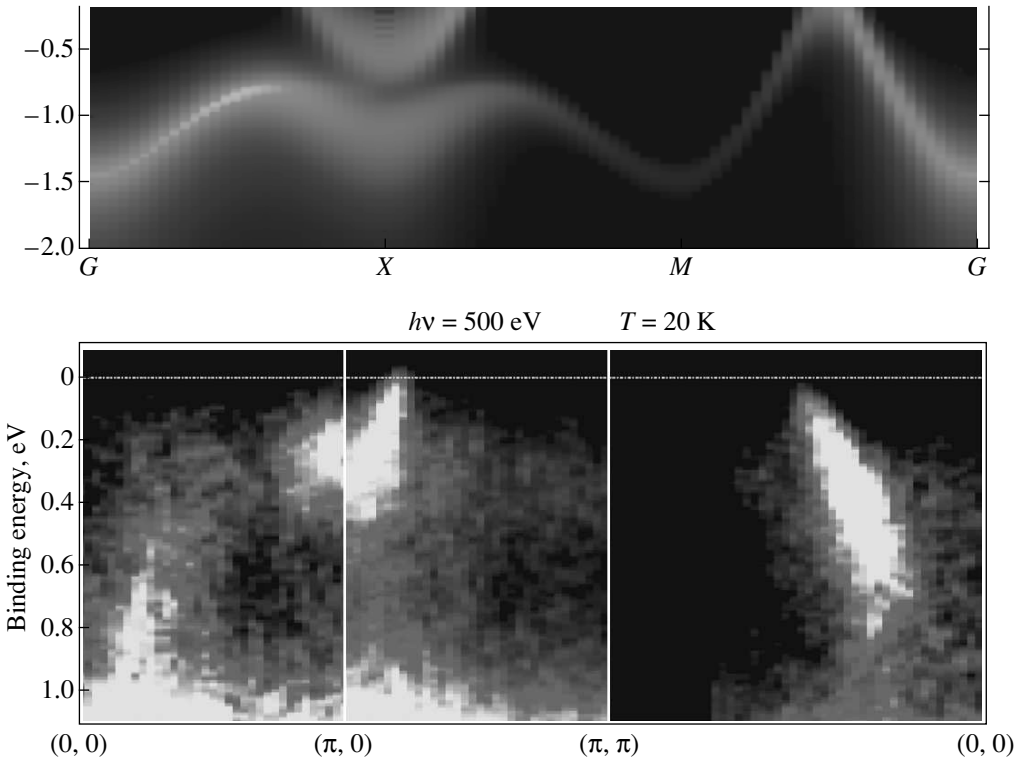

Fig. 8. Comparison of LDA+DMFT+$\Sigma_{\mathbf{k}}$ spectral functions (upper panel) for NCCO along the BZ high-symmetry directions with experimental ARPES data [37] (lower panel)

sults, namely, the observable physical quantities. This question arises from an ongoing scientific discussion in the literature. We note that our constrained LDA-calculated U value is of the order of 2–3t. At the same time, it is commonly believed that the U value should be of the order of 4–6t [29, 40]. For this, we have performed additional DMFT+$\Sigma_{\mathbf{k}}$ computations using these values of U.

If we just take higher values of U within the DMFT+$\Sigma_{\mathbf{k}}$ approach, without any change of other parameters of our model, we obtain a stronger uniform quasiparticle damping. Spectral functions become slightly more blurred and the FS less sharply defined. Also with the increase in the U value, the quasiparticle mass slightly increases. In the optical conductivity, the pseudogap anomaly also appears to be more damped, as we mentioned in Ref. [13]. At the same time, the general agreement with experiments stays reasonable. This is not very surprising because these values still belong to small or moderate correlations (U is less than the band width $W = 8t$).

But actually, we are trying to express the pseudogap potential Δ in terms of U (see Appendix). If this connection is taken into account, FS maps do not differ very much from those obtained above. However, the pseudogap effects become stronger both around "hot spots" and in the vicinity of the $(\pi/2a, \pi/2a)$ $\mathbf{k}$-point. In this case, comparison with ARPES data for quasiparticle bands becomes much worse. Especially, the larger U values spoil the agreement with optical data. Thus, we can conclude that the constrained LDA-calculated value of U (together with the corresponding value of Δ) allows describing ARPES experimental data reasonably well, although the size of the pseudogap in the optical conductivity is somewhat overestimated. In other respects, we do not observe any qualitative changes in our results as U increases from $3t$ to $4t$ or $6t$.

5. CONCLUSION

To summarize, the origin of evident "hot spots" on the NCCO FS in the pseudogap regime is attributed to the details of the noninteracting electron band structure of this compound. All differences in physical properties calculated within the LDA+DMFT+$\Sigma_{\mathbf{k}}$ approach (quasiparticle bands, FS maps, and ARPES data) are determined by the fact that "hot spots" lie

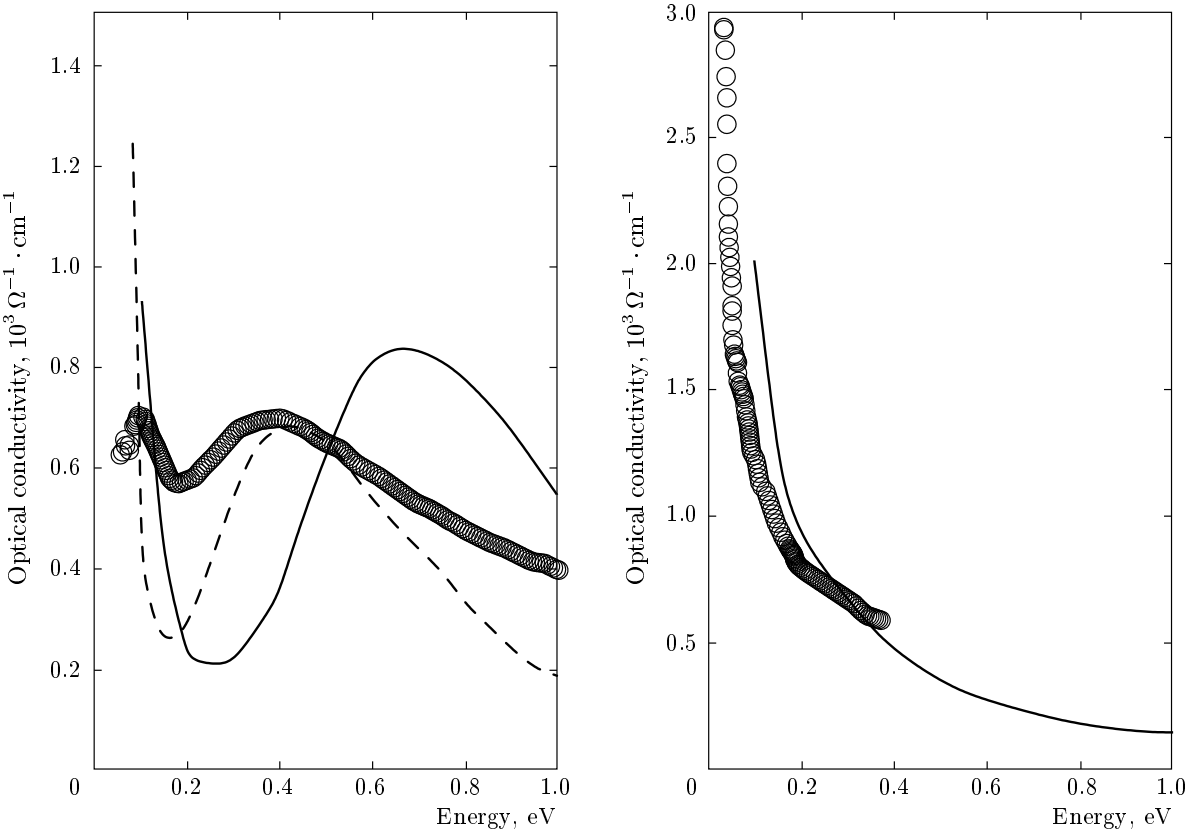

Fig. 9. Comparison of the LDA+DMFT+$\Sigma_{\mathbf{k}}$ calculated optical conductivity spectra for NCCO (left panel) with experimental data [38] (circles). Solid line shows theoretical results for the calculated pseudogap value $\Delta = 0.36$ eV (the dashed line corresponds to the experimental value $\Delta = 0.2$ eV). The right panel shows the same quantity for Bi2212 and the experiment in Ref. [39]

closer to the BZ center in NCCO than in Bi2212. Also a stronger AFM long-range ordering tendency in NCCO favors the clearly visible "hot spots". Apart from that, the qualitative behavior of both electron-doped NCCO and hole-doped Bi2212 high-T_c systems is almost the same. We have also interpreted the new ARPES experimental data for NCCO by the LDA+DMFT+$\Sigma_{\mathbf{k}}$ calculated quasiparticle bands and proposed a new mechanism for the origin of a van Hove-like singularity at -0.3 eV.

The results obtained yield further evidence that the LDA+DMFT+$\Sigma_{\mathbf{k}}$ approach is an efficient method to investigate the electron structure of strongly correlated systems.

We thank Thomas Pruschke for providing us with the NRG code and O. Jepsen for the helpful discussions. This work is supported by the RFBR grants 08-02-00021, 08-02-00712, and 08-02-91200, the RAS programs "Quantum macrophysics" and "Strongly correlated electrons in semiconductors, metals, superconductors, and magnetic materials", the Dynasty Foundation, Grants of the President of Russia MK-2242.2007.2, MK-3227.2008.2, SS-1929.2008.2, interdisciplinary UB-SB RAS project, the Russian Science Support Foundation. IN thanks the University of Osaka (Japan) for hospitality.

APPENDIX

Particle–Hole Asymmetry of the Pseudogap Potential Δ

The pseudogap energy scale (amplitude) Δ was calculated in Ref. [5] via DMFT (QMC, Quantum Monte Carlo) simulations for the hole-doped region. Here, we present similar results for the electron-doped case obtained with DMFT (NRG, numerical renormalization group). Using the two-particle self-consistent approach in Ref. [40], with the approximations introduced in

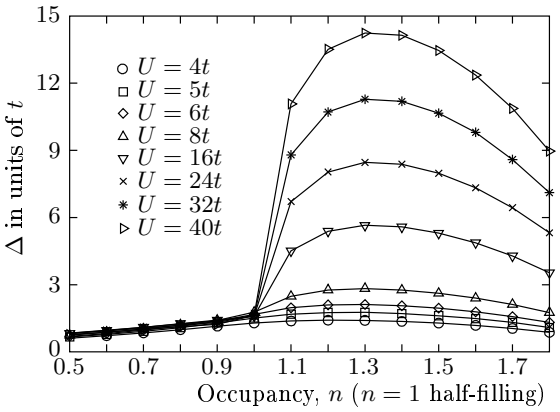

Fig. 10. Filling dependence of the pseudogap potential Δ calculated with DMFT(QMC) and DMFT(NRG) for a varying Coulomb interaction (U) at the temperature $T = 0.4t$ on a two-dimensional square lattice with $t'/t = -0.4$

Refs. [7, 8], we can derive the following microscopic expression for Δ in the standard Hubbard model:

$$\Delta^2 = U^2 \frac{\langle n_{i\uparrow} n_{i\downarrow}\rangle}{n^2} \langle (n_{i\uparrow} - n_{i\downarrow})^2 \rangle, \qquad \text{(A.1)}$$

where we take only scattering by antiferromagnetic spin fluctuations into account. The different local quantities here, such as the density n and the double occupancy $\langle n_{i\uparrow} n_{i\downarrow}\rangle$, can easily be calculated within the standard DMFT [3]. As the impurity solver, we used the NRG.

In Fig. 10, we show our results for Δ for both electron and hole dopings. We immediately see a remarkable (up to an order of magnitude) particle–hole asymmetry in Eq. (A.1) for large values of U. For values of U less than or equal to $8t$ (which corresponds to weak or moderate coupling), this Δ particle–hole asymmetry is about a factor of two. In the case of Eq. (A.1), it essentially comes from the particle–hole asymmetry of the double occupancy $\langle n_{i\uparrow} n_{i\downarrow}\rangle$ value, which is enhanced as the U value increases. These results agree with the experimental observation that pseudogap effects are stronger for electron-doped systems.

REFERENCES

1. T. Timusk and B. Statt, Rep. Progr. Phys. **62**, 61 (1999); M. V. Sadovskii, Usp. Fiz. Nauk **171**, 539 (2001) [Physics–Uspekhi **44**, 515 (2001)].

2. A. Damascelli, Z. Hussain, and Z.-X. Shen, Rev. Mod. Phys. **75**, 473 (2003); J. C. Campuzano, M. R. Norman, and M. Randeria, in "Physics of Superconductors", Vol. II, ed. K. H. Bennemann and J. B. Ketterson, Springer, Berlin (2004), p. 167; J. Fink et al., arXiv:cond-mat/0512307; X. J. Zhou et al., arXiv:cond-mat/0604284.

3. A. Georges, G. Kotliar, W. Krauth, and M. J. Rozenberg, Rev. Mod. Phys. **68**, 13 (1996).

4. E. Z. Kuchinskii, I. A. Nekrasov, and M. V. Sadovskii, JETP Lett. **82**, 198 (2005).

5. M. V. Sadovskii, I. A. Nekrasov, E. Z. Kuchinskii, Th. Prushke, and V. I. Anisimov, Phys. Rev. B **72**, 155105 (2005).

6. E. Z. Kuchinskii, I. A. Nekrasov, and M. V. Sadovskii, Low Temp. Phys. **32**, 528 (2006).

7. J. Schmalian, D. Pines, and B. Stojkovic, Phys. Rev. B **60**, 667 (1999).

8. E. Z. Kuchinskii and M. V. Sadovskii, Zh. Eksp. Teor. Fiz. **115**, 1765 (1999) [(JETP **88**, 347 (1999)].

9. R. O. Jones and O. Gunnarsson, Rev. Mod. Phys. **61**, 689 (1989).

10. K. Held, I. A. Nekrasov, G. Keller, V. Eyert, N. Blumer, A. K. McMahan, R. T. Scalettar, Th. Pruschke, V. I. Anisimov, and D. Vollhardt, Psi-k Newsletter **56**, 65 (2003) [psi-k.dl.ac.uk/newsletters/News_56/Highlight_56.pdf]; K. Held, Adv. Phys. **56**, 829 (2007).

11. K. G. Wilson, Rev. Mod. Phys. **47**, 773 (1975); H. R. Krishna-murthy, J. W. Wilkins, and K. G. Wilson, Phys. Rev. B **21**, 1003 (1980); Phys. Rev. B **21**, 1044 (1980); A. C. Hewson, *The Kondo Problem to Heavy Fermions*, Cambridge University Press (1993).

12. R. Bulla, A. C. Hewson, and Th. Pruschke, J. Phys.: Condens. Matter **10**, 8365 (1998).

13. E. Z. Kuchinskii, I. A. Nekrasov, and M. V. Sadovskii, Phys. Rev. B **75**, 115102 (2007).

14. E. Z. Kuchinskii, I. A. Nekrasov, and M. V. Sadovskii, Zh. Eksp. Teor. Fiz. **133**, 670 (2008).

15. E. Z. Kuchinskii, I. A. Nekrasov, Z. V. Pchelkina, and M. V. Sadovskii, JETP **104**, 792 (2007); I. A. Nekrasov, E. Z. Kuchinskii, Z. V. Pchelkina, and M. V. Sadovskii, Physica C **460–462**, 997 (2007).

16. M. V. Sadovskii, Zh. Eksp. Teor. Fiz. **77**, 2070 (1979) [JETP **50**, 989 (1979)].

17. M. V. Sadovskii and N. A. Strigina, Zh. Eksp. Teor. Fiz. **122**, 610 (2002) [JETP **95**, 526 (2002)].

18. J. M. Tarascon et al., Phys. Rev. B **37**, 9382 (1988); S. A. Sunshine et al., Phys. Rev. B **38**, 893 (1988).

19. T. Kamiuama, Physica C **229**, 377 (1994).

20. O. K. Anderson, Phys. Rev. B **12**, 3060 (1975); O. K. Andersen and O. Jepsen, Phys. Rev. Lett. **53**, 2571 (1984).

21. M. Hybertsen and L. Mattheiss, Phys. Rev. Lett. **60**, 1661 (1988).

22. S. Massidda, N. Hamada, Jaejun Yu, and A. J. Freeman, Physica C **157**, 571 (1989); S. Matsuno and H. Kanimura, J. Supercond. **7**, 517 (1994).

23. N. Marzari and D. Vanderbilt, Phys. Rev. B **56**, 12847 (1997); Wei Ku, H. Rosner, W. E. Pickett, and R. T. Scalettar, Phys. Rev. Lett. **89**, 167204 (2002).

24. V. I. Anisimov, D. E. Kondakov, A. V. Kozhevnikov, I. A. Nekrasov, Z. V. Pchelkina, J. W. Allen, S.-K. Mo, H.-D. Kim, P. Metcalf, S. Suga, A. Sekiyama, G. Keller, I. Leonov, X. Ren, and D. Vollhardt, Phys. Rev. B **71**, 125119 (2005).

25. O. K. Andersen and T. Saha-Dasgupta, Phys. Rev. B **62**, R16219 (2000); O. K. Andersen, T. Saha-Dasgupta, S. Ezhov, L. Tsetseris, O. Jepsen, R. W. Tank, C. Arcangeli, and G. Krier, Psi-k Newsletter **45**, 86 (2001); O. K. Andersen, T. Saha-Dasgupta, and S. Ezhov, Bull. Mater. Sci. **26**, 19 (2003).

26. M. Korshunov, A. Gavrichkov, S. G. Ovchinnikov, Z. V. Pchelkina, I. A. Nekrasov, M. A. Korotin, and V. I. Anisimov, J. Exp. and Theor. Phys. **99**, 559 (2004); M. M. Korshunov, V. A. Gavrichkov, S. G. Ovchinnikov, I. A. Nekrasov, E. E. Kokorina, and Z. V. Pchelkina, J. Phys.: Condens. Matter **19**, 486203 (2007).

27. O. K. Andersen, A. I. Liechtenstein, O. Jepsen, and F. Paulsen, J. Phys. Chem. Sol. **56**, 1573 (1995).

28. O. Gunnarsson, O. K. Andersen, O. Jepsen, and J. Zaanen, Phys. Rev. B **39**, 1708 (1989).

29. N. M. Plakida and V. S. Oudovenko, JETP **104**, 230 (2007).

30. I. A. Nekrasov, K. Held, N. Blümer, A. I. Poteryaev, V. I. Anisimov, and D. Vollhardt, Eur. Phys. J. B **18**, 55 (2000).

31. I. A. Zobkalo, A. G. Gukasov, S. Yu. Kokovin, S. N. Barilo, and D. I. Zhigunov, Sol. St. Comm. **80**, 921 (1991); E. M. Motoyama, G. Yu, I. M. Vishik, O. P. Vajk, P. K. Mang, and M. Greven, Nature **445**, 186 (2007).

32. M. V. Sadovskii, E. Z. Kuchinskii, and I. A. Nekrasov, Physica C **460–462**, 1084 (2007).

33. N. P. Armitage, F. Ronning, D. H. Lu, C. Kim, A. Damascelli, K. M. Shen, D. L. Feng, H. Eisaki, Z.-X. Shen, P. K. Mang, N. Kaneko, M. Greven, Y. Onose, Y. Taguchi, and Y. Tokura, Phys. Rev. Lett. **88**, 257001 (2002).

34. A. Kaminski, H. M. Fretwell, M. R. Norman, M. Randeria, S. Rosenkranz, U. Chatterjee, J. C. Campuzano, J. Mesot, T. Sato, T. Takahashi, T. Terashima, M. Takano, K. Kadowaki, Z. Z. Li, and H. Raffy, Phys. Rev. B **88**, 257001 (2002).

35. I. A. Nekrasov, E. E. Kokorina, E. Z. Kuchinskii, Z. V. Pchelkina, and M. V. Sadovskii, arXiv:0708.2313.

36. S. V. Borisenko, M. S. Golden, S. Legner, T. Pichler, C. Drr, M. Knupfer, J. Fink, G. Yang, S. Abell, and H. Berger, Phys. Rev. Lett. **84**, 4453 (2000).

37. M. Tsunekawa, A. Sekiyama, S. Kasai, A. Yamasaki, H. Fujiwara, M. Sing, A. Shigemoto, S. Imada, Y. Onose, Y. Tokura, T. Muro, and S. Suga, J. Electr. Spectr. Rel. Phen. **144–147**, 541 (2005); M. Tsunekawa, A. Sekiyama, S. Kasai, A. Imada, H. Fujiwara, M. Muro, Y. Onose, Y. Tokura, and S. Suga, New J. Phys. **10**, 073005 (2008).

38. Y. Onose, Y. Taguchi, K. Ishizaka, and Y. Tokura, Phys. Rev. Lett. **87**, 217001 (2001).

39. M. A. Quijada, D. B. Tanner, R. J. Kelley, M. Onellion, H. Berger, and G. Margaritondo, Phys. Rev. B **60**, 14917 (1999).

40. Y. M. Vilk and A.-M. S. Tremblay, J. de Phys. I **7**, 1309 (1997).